

This is the accepted manuscript made available via CHORUS. The article has been published as:

Laboratory study of avalanches in magnetized plasmas

B. Van Compernelle, G. J. Morales, J. E. Maggs, and R. D. Sydora

Phys. Rev. E **91**, 031102 — Published 11 March 2015

DOI: [10.1103/PhysRevE.91.031102](https://doi.org/10.1103/PhysRevE.91.031102)

Laboratory study of avalanches in magnetized plasmas

B. Van Compernelle,^{1,*} G. J. Morales,¹ J. E. Maggs,¹ and R. D. Sydora²

¹*Physics and Astronomy Department, University of California Los Angeles, Los Angeles, CA 90095*

²*Department of Physics, University of Alberta, Edmonton AB T6G 2E1, Canada*

(Dated: February 18, 2015)

It is demonstrated that a novel heating configuration applied to a large and cold magnetized plasma allows the study of avalanche phenomena under controlled conditions. Intermittent collapses of the plasma pressure profile, associated with unstable drift-Alfvén waves, exhibit a two-slope power-law spectrum with exponents near -1 at lower frequencies and in the range of -2 to -4 at higher frequencies. A detailed mapping of the spatio-temporal evolution of a single avalanche event is presented.

PACS numbers: 52.25Fi, 52.35.Kt, 52.35Ra

Avalanches are sudden events that are initially localized but can cause major, long-term changes over an extended region of a physical system [1]. Although the concept is commonly associated with catastrophic snow avalanches [2], the general phenomena occurs widely in nature [3, 4] and in devices built by humans [5, 6]. The origin of the various manifestations of avalanches is the presence of a steep gradient in one of the parameters that categorize the underlying system. Often there is a threshold value for the gradient; when it is exceeded, a complex sequence of processes is triggered whose ultimate role is to relax the gradient below the threshold value. For cases in which the triggered process attains a relatively large amplitude level, the system can be irreversibly destroyed. But in other important situations, external agents are present that reestablish the gradient, which can then, again, exceed the threshold value. In this environment a sequence of avalanches is generated, but the actual time of occurrence of an individual event displays a marked degree of unpredictability. In this sense, the behavior is intermittent and causes the parameters of the system to evolve from place to place, i.e., there is an associated transport that occurs.

This Letter reports on avalanche phenomena in magnetized plasmas triggered by gradients in plasma temperature and density across the magnetic field. The vast majority of experimental information about plasmas that exhibit cross-field avalanches has been obtained in confinement devices designed for fusion studies [7–10]. Due to the complexity of the magnetic topology, multiple heating and fueling scenarios, and interactions with boundaries, these devices provide a difficult environment in which to unravel the subtle mechanisms, e.g., self-organized-criticality (SOC) [11–16] and streamers [17–20], among others, that have been extensively investigated in theoretical and modeling studies [21–29] by the plasma community. This Letter significantly expands the basic experimental information available by exploring the behavior of a well-defined plasma configuration that exhibits avalanches.

The experiment is performed on the upgraded Large

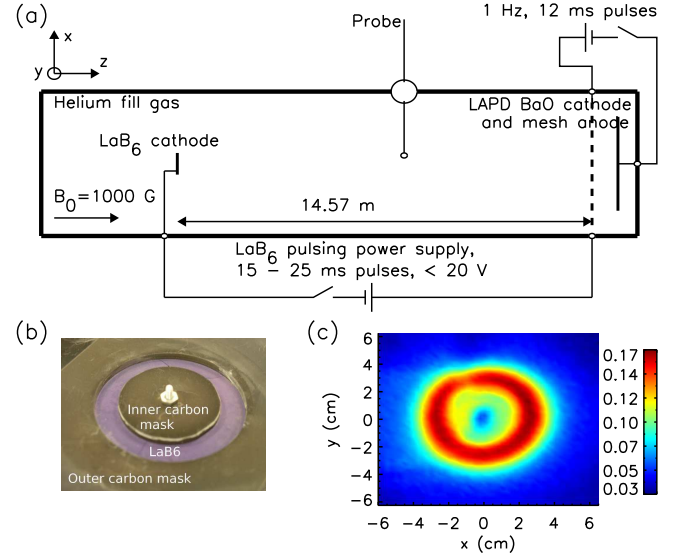


FIG. 1. (Color online) (a) Schematic of the experimental setup, not to scale. A ring-shaped LaB₆ cathode injects low-energy electrons into a large cold magnetized plasma, which acts as an ideal, hollow and cylindrical heat source. (b) Front end of cathode assembly. (c) 2D cross-field ion saturation current profile.

Plasma Device (LAPD) [30, 31] at the Basic Plasma Science Facility (BaPSF) at UCLA. The LAPD is a cylindrical device, with axial magnetic field that confines a quiescent plasma column 18 m long and 60 cm in diameter. The plasma is created from collisional ionization of He gas by the fast electrons of a large area electron beam, produced by the application of a positive voltage between a barium oxide (BaO) coated cathode and a mesh anode 50 cm away. The electron beam heats the plasma to electron temperatures in the range of 5 eV and creates electron densities of a few times 10^{12} cm^{-3} . The active phase lasts for 10 milliseconds and is repeated every second (1 Hz pulse rate). The avalanche experiment is performed in the afterglow phase, after the active phase of the LAPD discharge is turned off. In the afterglow phase, electron

temperatures fall below 0.5 eV within 100 microseconds while densities remain in the range of 10^{12} cm^{-3} . The density decreases exponentially with a time constant of tens of milliseconds while the avalanche experiment lasts 15–25 milliseconds.

A secondary cathode [32], made of lanthanum hexaboride (LaB_6), is inserted into the machine at the opposite end of the BaO coated cathode, as shown in Fig. 1(a). LaB_6 is a refractory ceramic material with a low work function, around 2.5 eV, and has one of the highest known electron emissivities when heated to its operating temperature in the range of 1800 K. The front side of the LaB_6 disk is masked by carbon plates to leave a ring of exposed LaB_6 with 4 cm inner diameter and 6 cm outer diameter, as in Fig. 1(b). When the LaB_6 disk is biased with respect to an axially distant anode, electrons are emitted from the LaB_6 in the form of a hollow cylindrical 'ring'. Beam electrons, injected into afterglow plasmas in LAPD with energies below ionization energy, are slowed down by Coulomb collisions over a region along the magnetic field about 1/10 the machine length. The slowing down region acts as an ideal heat source that raises the temperature of the cold background plasma. The ring source thus produces a hollow, cylindrical heated region embedded in the background cold plasma. Emission currents of the LaB_6 cathode are in the range of a few amperes. The temperature of the cold background plasma rises from less than 0.5 eV to 5 eV within the hollow ring region that maps along magnetic lines to the LaB_6 disk. Heating power is controlled by setting the discharge voltage. The heating power per particle effectively increases in time during the experiment as the plasma density slowly decays due to the lack of ionization. The confining magnetic field strength in this experiment is 1000 G.

The plasma is diagnosed with Langmuir probes measuring ion saturation current. The current collected by the probe is proportional to $n_e \sqrt{T_e}$, where n_e is the electron plasma density and T_e is the electron temperature. LAPD has probe access every 32.5 cm along the magnetic field direction. Probes are mounted on computer controlled probe drives connected to ball valves [33] enabling 3D measurements of plasma parameters. Typically, a probe moves through a series of user-defined positions at fixed axial location. At each position, data from several plasma shots is acquired and stored, before moving to the next position. Since the LAPD plasma is highly reproducible, an ensemble of plasma parameter measurements can thus be obtained in a 2D plane at fixed axial location. Additional fixed-probes are used as a reference for cross-correlation analysis or conditional averaging.

Figure 1(c) shows a 2D contour of the measured ion saturation current, in a cross section perpendicular to the magnetic field at an axial distance of 3.6 m from the LaB_6 source. Three distinct regions can be identified in the ra-

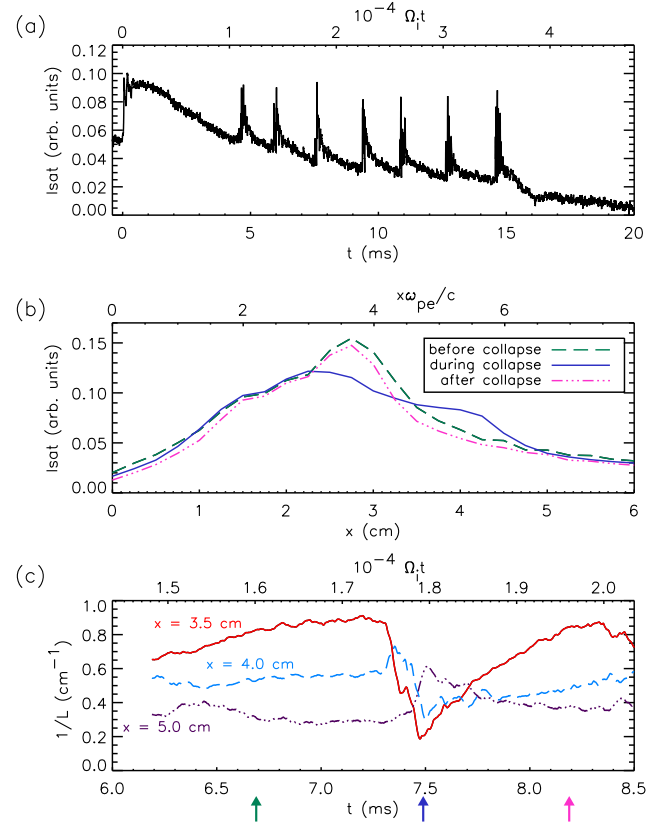


FIG. 2. (Color online) (a) Characteristic time trace of ion saturation current on the outer gradient region. The 'spikes' represent avalanche events. The LaB_6 source is on for 15 ms. (b) Radial profile modification at fixed azimuthal position during one avalanche event, at $t = 6.69$ ms, $t = 7.49$ ms and $t = 8.19$ ms; data is low-pass filtered below frequencies associated with azimuthal fluctuations. (c) Time evolution of inverse of the gradient scale length at 3 locations on the outer region. Arrows indicate times at which radial profiles are shown in panel (b).

dial profile: the inner gradient; the ring filament; and the outer gradient. The ring filament is the region that directly maps along magnetic field lines to the ring-shaped LaB_6 source; it is where the plasma pressure peaks.

Figure 2(a) shows the characteristic evolution at a radial position on the outer gradient region. Time traces exhibit intermittent positive pulses, which are accompanied by a decrease (negative pulses) in the plasma pressure within the heated region, thereby collapsing the pressure profile in the outer region. The inner gradient region does not exhibit pulses and remains quiescent. These 'spikes', or pulses, in ion saturation current are the signature of an avalanche event. After each pulse the system slowly recovers to the baseline ion saturation current until the next pulse occurs. The monotonic decrease in the mean value (or baseline) of the signal in Fig. 2(a) is due to the natural decay of the plasma density in the afterglow phase. The positive pulses, however, have similar

amplitudes indicating that the profile collapses become more severe as time progresses. This is a consequence of the increase in the effective heating power per-particle along the heated field lines as the density decays while the LaB₆ discharge power remains fixed. Increasing the LaB₆ discharge power, for the same initial density value, results in the avalanche pulses having larger amplitude as well as a larger radial extent.

The time at which an individual avalanche occurs has an unpredictable nature and varies from shot to shot. To overcome this variability, a fixed reference probe, positioned axially downstream or upstream from where the ion saturation current is collected, is used to provide a 'timing reference' of an avalanche event for every plasma shot. For each plasma shot, the occurrence time t_0 of a local maximum in the drift-wave fluctuations is identified near the maximum of each avalanche/spike collected by the reference probe. The data on the moving and reference probes is retained and saved, for 1 ms before t_0 and after t_0 , for each avalanche event. The time t_0 is then effectively the time origin for all signals associated with the selected avalanche event. This allows for the reconstruction, spatially and temporally, of the evolution of the avalanches. Fig. 2(b-c) illustrate the sequence of profile modifications associated with one avalanche event. The measurement is made at a fixed azimuthal position and a low-pass frequency filter is applied to remove azimuthal fluctuations. Radial profiles of ion saturation current are shown in Fig. 2(b) for time intervals before, during and after the avalanche. The avalanche collapses the outer gradient, but the inner gradient is unperturbed. The ion saturation current profiles return to their pre-avalanche shape approximately within 1 ms after the gradient is modified.

The time evolution of the inverse of the gradient scale length, i.e., $1/L = d/dx \ln(I_{sat})$, at three radial positions on the outer region is shown in Fig. 2(c); it illustrates the connection of an avalanche to the steepness of the profile. It is seen that the largest gradient, initially located at $x = 3.5$ cm, increases steadily in time due to the external heating and it undergoes a rapid collapse around $t = 7.3$ ms, i.e., the scale-length increases by a factor of 4 within 150 μ s. But at $x = 4.0$ cm, where the gradient is initially smaller, there is a rapid decrease in the scale-length followed by another collapse. This is a signature of a steep avalanche front moving out radially. The radial velocity is on the order of 0.8×10^4 cm/s which is two orders of magnitude less than the sound speed ($c_s = 5 \times 10^5$ cm/s). After the avalanche front passes by, the local gradient recovers on a slower time scale to its pre-avalanche value. At the larger radial position, $x = 5.0$ cm, the avalanche pulse arrives later in time and the relaxation is slower. The recovery time, on the order of 0.5 ms, is determined by the heating source and by the thermal conductivity.

Figure 3(a) displays the frequency power spectrum in log-log format for signals measured by the reference probe

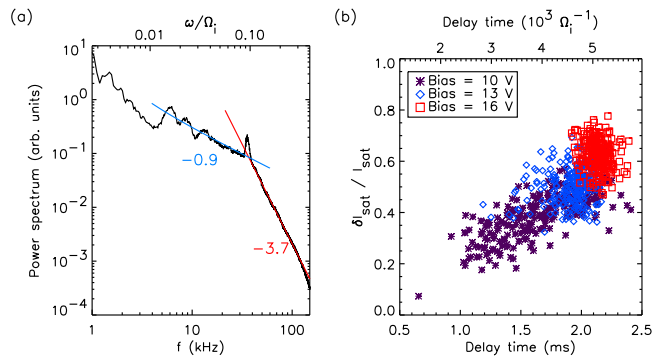


FIG. 3. (Color online) (a) Power spectrum over a time window encompassing 4 - 6 avalanches and averaged over 500 plasma shots, (b) Statistical behavior of the relative amplitude of a second avalanche and its delay time from an earlier one. Delay time is between first and second avalanche in each plasma shot, and amplitude is measured relative to the decaying baseline value. Results of three different heating powers are shown.

at a radius $r = 4.0$ cm and 3.2 m axial distance from the LaB₆ source. The spectrum exhibits power-law behavior within two distinct regions. At high frequencies a large power-law exponent is measured, -3.7 in this case. There is a clear line spectral component near 30 kHz, which is also where a break in the power-law spectrum is visible. The power-law exponent at frequencies below the break is close to -1 and its value is insensitive to changes in heating power. However, the power-law exponent at higher frequencies varies with heating power, ranging from -2 to -4 as the heating power is increased. The power-spectrum of the measured avalanches shows strong similarities with power-law spectra obtained in numerical studies that enlarge the concept of self-organized-criticality to include finite driving forces [13] and mixed diffusive dynamics [23], which predict two-sloped power-law spectra with exponents in the range of -2 to -4 at the higher frequencies and exponents near -1 at the lower frequencies.

Statistical properties of the avalanches are presented in Fig. 3(b). Time series measured by the reference probe are used to quantify the time delay between successive avalanches as well as the size of avalanches. The amplitude relative to the baseline level before an avalanche onset is chosen in order to compensate for the density decay of the background plasma and the different times at which individual avalanches occur. The scatter plot in Fig. 3(b) shows the variation in both the delay time between the first and second avalanche in each time trace, and the relative size of the second avalanche. A clear trend is observed for three source bias voltages (heating powers); large time delays are followed by stronger avalanches. The higher heating powers in general also result in larger avalanches.

The dynamical range of the size of the avalanches and the dynamical range of the waiting time between

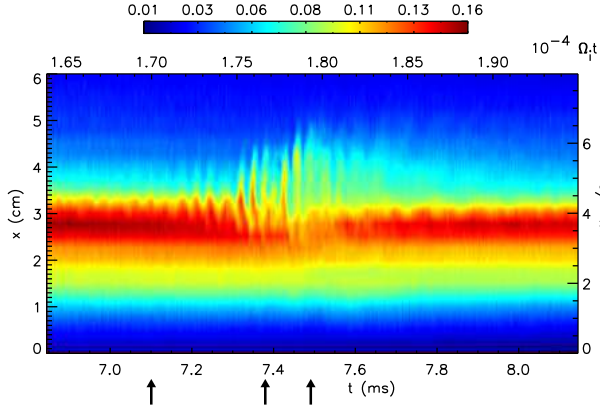


FIG. 4. (Color online) Radial and temporal structure of one avalanche event. Arrows indicate times at which the 2D structure is shown in Fig. 5.

avalanches is relatively small for a given heating power, as is apparent from Fig. 2(a) and Fig. 3(b). The avalanches observed in the experiment are all global avalanches, in the sense that they collapse the profile in the whole outer gradient region, and they occur at nearly regular intervals. Partial collapses of the profile in the outer gradient region are not seen. Similar results were obtained by Nagel [14] in laboratory experiments of sandpiles. This behavior is in contrast with avalanche models invoking self-organized-criticality which predicts avalanches at all spatial scales, and accompanied by a large range of waiting times, i.e., SOC predicts frequent small avalanches and rare large global events. The power-law probability distribution function of avalanche sizes and waiting times, predicted by SOC, cannot be checked in the experiment because the dynamical range exhibited by the magnetized plasma is too limited.

The origin of the line spectral component in the power spectrum of Fig. 3(a) is evident in Fig. 4, which displays the reconstruction of a single avalanche event as a contour plot of radial position versus time. The avalanche exhibits 2 dynamic scales, fast fluctuations with frequency in the 30 kHz range, and a collapse/recovery phase having a time-scale of hundreds of μ s. The 30 kHz fluctuations are attributed to drift-Alfvén waves [34]. Gyrokinetic simulations show linear growth of drift Alfvén waves for the experimental conditions. From the radial velocity of the avalanche front, $v_r = 0.8 \times 10^4$ cm/s, the potential fluctuations in the drift wave are estimated to be on the order of $e\Phi/T_e \simeq 0.06$. The drift modes are first seen at the point of largest gradient. As the wave amplitude grows the radial extent of the fluctuations increases and cause the average (near DC) ion saturation current in the heated region to drop. Approximately, about the same time, the fluctuations reach radial positions beyond the point where the mean gradient is largest; at these outer locations the average value of the ion saturation current increases. Once the pressure gradient is relaxed, the fluc-

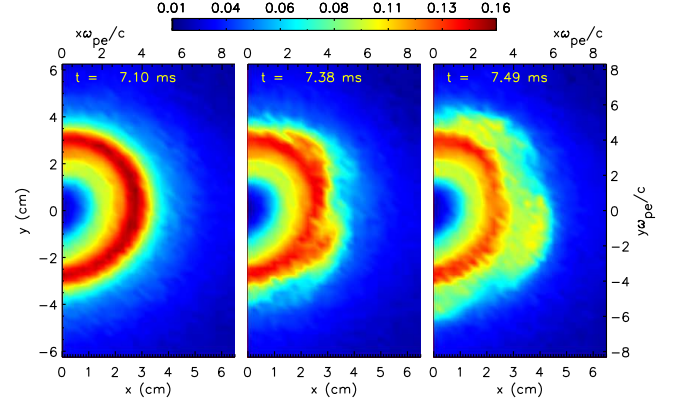


FIG. 5. (Color online) Radial and azimuthal structure of the heated region at three times during one avalanche event, indicated by arrows in Fig. 4. Left panel: before the onset, middle panel: early stages of profile collapse, right panel: late stages of profile collapse.

tuations disappear and the ion saturation current enters the recovery phase.

Figure 5 illustrates the azimuthal dependence of the drift mode fluctuations at three different times, before the onset of the avalanche, during the initial part of the profile collapse and during the late stage of the profile collapse. Before the onset of the avalanche the profile is stable and quiescent (left panel). Drift modes grow on the outer gradient during the initial stage of the avalanche, and the profile develops 'arms' sharply localized in the azimuthal direction (middle panel). The arms have an $m = 5$ azimuthal dependence and propagate in the electron diamagnetic direction. Several drift wave cycles later the remnants of these arms are seen to have moved out radially (right panel). The radial velocity of the arms is an order of magnitude lower than the azimuthal velocity, on the order of 1.3×10^5 cm/s. This corresponds to a radial displacement in the range of one fifth of the pre-avalanche mean gradient scale-length in one wave period. This is also evident from Fig. 4 which shows that the profile collapse happens within about six wave cycles. After the collapse the profile recovers to its initial shape.

In summary, avalanches in magnetized plasmas triggered by cross-field pressure gradients have been created in a controlled laboratory setting. The use of reference probes as time markers has allowed for the first time the visualization of the spatio-temporal evolution of the avalanche process. The measured spectral signatures display characteristic signatures consistent with studies that incorporate finite driving forces and mixed diffusive dynamics into the phenomenology of self-organized-criticality. The prediction of avalanches occurring at all spatial scales is not observed.

The authors wish to thank T.A. Carter for stimulating discussions and Z. Lucky and M. Drandell for their technical assistance. Work was done at the Basic Plasma

Science Facility (BAPSF) funded by DOE/NSF.

* bvcomper@physics.ucla.edu

- [1] K. Hutter, in *Hydrology of Disasters*, Vol. 24, edited by V. Singh (Springer Netherlands, 1996) pp. 317–394.
- [2] J. Schweizer, J. Bruce Jamieson, and M. Schneebeli, *Reviews of Geophysics* **41**, 1016 (2003).
- [3] W. Hager, S. J. Linz, and P. Hanggi, *EPL (Europhysics Letters)* **40**, 393 (1997).
- [4] E. T. Lu, R. J. Hamilton, J. M. McTiernan, and K. R. Bromund, *Astrophys. J.* **412**, 841 (1993).
- [5] S. Cova, A. Lacaita, and G. Ripamonti, *Electron Device Letters, IEEE* **12**, 685 (1991).
- [6] A. Sharoni, J. G. Ramírez, and I. K. Schuller, *Phys. Rev. Lett.* **101**, 026404 (2008).
- [7] P. A. Politzer, *Phys. Rev. Lett.* **84**, 1192 (2000).
- [8] P. A. Politzer, M. E. Austin, M. Gilmore, G. R. McKee, T. L. Rhodes, C. X. Yu, E. J. Doyle, T. E. Evans, and R. A. Moyere, *Phys. Plasmas* **9**, 1962 (2002).
- [9] V. Antoni, V. Carbone, R. Cavazzana, G. Regnoli, N. Vianello, E. Spada, L. Fattorini, E. Martines, G. Serrianni, M. Spolaore, L. Tramontin, and P. Veltri, *Phys. Rev. Lett.* **87**, 045001 (2001).
- [10] L. García, B. A. Carreras, and D. E. Newman, *Phys. Plasmas* **9**, 841 (2002).
- [11] H. J. Jensen, in *Self-Organized Criticality, Emergent Complex Behavior in Physical and Biological Systems* (Cambridge University Press, 1998).
- [12] P. Bak, C. Tang, and K. Wiesenfeld, *Phys. Rev. Lett.* **59**, 381 (1987).
- [13] T. Hwa and M. Kardar, *Phys. Rev. A* **45**, 7002 (1992).
- [14] S. R. Nagel, *Rev. Mod. Phys.* **64**, 321 (1992).
- [15] Y. Kishimoto, T. Tajima, W. Horton, M. J. LeBrun, and J. Y. Kim, *Phys. Plasmas* **3**, 1289 (1996).
- [16] D. E. Newman, B. A. Carreras, P. H. Diamond, and T. S. Hahm, *Phys. Plasmas* **3**, 1858 (1996).
- [17] P. H. Diamond and T. S. Hahm, *Phys. Plasmas* **2**, 3640 (1995).
- [18] X. Garbet and R. E. Waltz, *Phys. Plasmas* **5**, 2836 (1998).
- [19] P. Beyer, S. Benkadda, X. Garbet, and P. H. Diamond, *Phys. Rev. Lett.* **85**, 4892 (2000).
- [20] P. Diamond, S. Champeaux, M. Malkov, A. Das, I. Gruzinov, M. Rosenbluth, C. Holland, B. Wecht, A. Smolyakov, F. Hinton, Z. Lin, and T. Hahm, *Nuclear Fusion* **41**, 1067 (2001).
- [21] R. O. Dendy and P. Helander, *Phys. Rev. E* **57**, 3641 (1998).
- [22] Y. Sarazin, X. Garbet, P. Ghendrih, and S. Benkadda, *Phys. Plasmas* **7**, 1085 (2000).
- [23] R. Sánchez, D. Newman, and B. Carreras, *Nuclear Fusion* **41**, 247 (2001).
- [24] S. C. Chapman, R. O. Dendy, and B. Hnat, *Phys. Plasmas* **8**, 1969 (2001).
- [25] D. E. Newman, R. Sánchez, B. A. Carreras, and W. Ferenbaugh, *Phys. Rev. Lett.* **88**, 204304 (2002).
- [26] L. García and B. A. Carreras, *Phys. Plasmas* **12**, 092305 (2005).
- [27] J. A. Mier, L. García, and R. Sánchez, *Phys. Plasmas* **13**, 102308 (2006).
- [28] S. Tokunaga, H. Jhang, S. S. Kim, and P. H. Diamond, *Phys. Plasmas* **19**, 092303 (2012).
- [29] S. Jolliet and Y. Idomura, *Nuclear Fusion* **52**, 023026 (2012).
- [30] W. Geckelman, H. Pfister, Z. Lucky, J. Bamber, D. Leneman, and J. Maggs, *Rev. Sci. Instrum.* **62**, 2875 (1991).
- [31] D. Leneman, W. Geckelman, and J. Maggs, *Rev. Sci. Instrum.* **77**, 015108 (2006).
- [32] B. Van Compernelle, W. Geckelman, P. Pribyl, and C. Cooper, *Phys. Plasmas* **18**, 123501 (2011).
- [33] D. Leneman and W. Geckelman, *Rev. Sci. Instrum.* **72**, 3473 (2001).
- [34] J. R. Peñano, G. J. Morales, and J. E. Maggs, *Phys. Plasmas* **7**, 144 (2000).